IEEE Transactions on Transportation Electrification, Available online 16 July 2024
DOI: 10.1109/TTE.2024.3429202

Battery thermal management for microchannel cooling system with scanning flow method

Qing Qin, Zhenhua Luo, and Patrick Luk, *Member, IEEE*

***Abstract*— The demand for high-performance electric vehicles has rapidly increased, necessitating rapid charging and efficient thermal battery management. High-energy-density batteries generate massive heat impacting performance, service life and safety. Thermal management plays a critical role in preserving battery integrity by regulating overall temperature and localized heat distribution, thus mitigating the risk of thermal runaway. Varies cooling technologies such as air, liquid, and multi-phase material cooling, have been utilized. However, minimizing the maximum temperature while maintaining temperature uniformity remains a critical challenge in battery thermal management. This paper introduces a novel microchannel cooling system with scanning flow for Li-ion batteries. Computational Fluid Dynamics (CFD) models are developed to investigate scanning flow cooling behavior. Parametric study examines the effects of battery numbers, valve switching frequency, and channel numbers on maximum and minimum temperatures, average temperature, and temperature differences. Furthermore, fluid analysis incorporates heat distribution and velocity behavior to study flow characteristics. Experimental analysis validates the cooling capability of the scanning flow method with a 0.17% error rate. The findings highlight scanning flow as an efficient method, enhancing temperature uniformity by 62.5% and reducing the average temperature difference by 92%. This presents a promising avenue for developing effective thermal management solutions for high-energy-density batteries.**

***Index Terms*—Cooling, battery, liquid cooling, temperature control**

I. INTRODUCTION

THE ongoing global shift toward electrified transportation is being facilitated by the advancement and deployment of electric vehicles (EVs). The presence of fast charging can mitigate concerns related to charging duration and range anxiety, representing two pivotal impediments hindering the widespread embrace of electric vehicles [1]. Current EVs predominantly depend on residential and workplace charging facilities denoted as level 1 and level 2, with several hours of charging duration [2]. Consequently, the implementation of high-energy-density batteries capable of rapid charging has emerged as a desirable goal for EVs. Nevertheless, it is important to note that rapid charging, which involves high current rates, accentuates the importance of effective battery thermal management [3].

The battery generates heat during charge and discharge due to enthalpy changes, electrochemical polarization and resistive heating within the cell [4]. This heat has a substantial impact on the operational temperature of the battery, thereby significantly influencing its charging and discharging performance, internal electrochemical reactions, service life, and safety [5]. Moreover, temperature fluctuations within batteries can cause uneven temperature distribution, impacting charging and discharging behavior [6], emphasizing the need for enhanced battery thermal management systems. Common cooling methods for electric vehicles include air cooling, liquid cooling, phase-changing material (PCM) cooling, and thermoelectric cooling [7]. While air cooling does have a certain impact on lowering battery pack temperatures, it is accompanied by the drawback of generating noise. PCM cooling shows promising cooling during phase-changing transitions but its effectiveness decreases afterward [8]. In contrast, thermoelectric cooling is highly reliable, featuring no moving mechanical parts or liquid components, but it is characterized by elevated costs and limited energy efficiency [9]. Among these cooling methods, liquid cooling has emerged as the most widely utilized cooling approach in EVs.

A liquid cooling system is more effective than air cooling due to the superior thermal conductivity and heat-carrying capacity exhibited by liquids. The liquid cooling system can be categorized into indirect liquid cooling and direct liquid cooling by the contact of the battery cells. The direct cooling system is the liquid directly in contact with the battery surface. Guo et al. [10] proposed a lightweight multi-channel liquid cooling system for pouch Lithium-ion batteries. Their multi-objective optimization decreased accessory mass by 10.25% and capped the maximum temperature at 36°C during 3C discharging. The liquid in indirect cooling has no direct contact with the battery cell surface, which is widely used in applications. Han et al. [11] proposed and compared several fin structures with circular, rectangular and triangular shapes for the dielectric fluid immersion cooling system to improve the evenness of liquid flow by numerical and experimental methods. Their results showed that the maximum temperature of the battery pack is lowered by 2.41%, 2.57% and 4.45% for circular, rectangular and triangular fin structures. Nevertheless, the temperature difference between the battery cells near the inlet and outlet was still observed. Xu et al [12] demonstrated an indirect cooling with an optimized U shape cooling channel to minimize the maximum temperature difference (MTD) of the automotive lithium battery pack. Their simulation results illustrated that the maximum temperature difference is reduced by 7.49%.

In addition to integrating cooling channel structures, controlling flow behavior, such as the application of pulsatile

This work was supported by Engineering and Physical Sciences Research Council. *Corresponding author: Patrick Luk.*

The authors are with Center for Energy Engineering, Cranfield University, Cranfield, MK43 0AL UK(e-mail: P.C.K.Luk@Cranfield.ac.uk).

Color versions of one or more of the figures in this article are available online at http://ieeexplore.ieee.org

flow (also called pulsating flow), represents another method for enhancing the cooling effect of battery thermal management systems. Pulsatile flow is a unique flow phenomenon with uncertain fluctuation widespread in nature, such as the blood flow in vessel. The pumping mechanism of the heat generates a pulsatile pressure gradient that generates a regulated pulse through the blood flow in the human circulatory system [13]. Pulsatile flow is widely applied in engineering and Bio-medical applications for various uses [14], [15]. Furthermore, owing to its superior heat transfer enhancement, pulsatile flow is applied in thermal management applications such as internal combustion and Stirling engines [16], [17], heat exchangers [18], and pulsating heat pipes[19]. The study for pulsating flow mainly uses laminar flow at the inlet [20], [21]. When pulsating flow is introduced into a continuous flow, it alters the characteristics of the boundary layer, consequently modifying the thermal resistance. In fact, the velocity profile for pulsating flow exhibits a greater uniformity when contrasted with steady flow, leading to an increase in heat transfer when pulsating flow is enabled [15]. pulsating flow has the capability to induce turbulence, which effectively blends high and low-temperature fluids, thereby augmenting heat transfer [22]. Furthermore, authors previously[23]–[25] applied pulsating flow cooling to active garments using a high-frequency electromagnetic micro pump, offering flexibility to allow personalized temperature conditions. Experimental results demonstrate the pulsating flow system has a faster cooling effect and overall better cooling than conventional continuous flow.

Despite the limited number of studies applying pulsatile flow in battery thermal management, this is primarily due to the novelty of this approach within the field. Li et al.[26] introduced a multi-channel cold plate thermal management system for pouch cell batteries utilizing pulsating flow, controlled by a single valve. The pulsating flow operates simultaneously in all pipes. Their findings indicated a 5% reduction in energy consumption compared to steady flow conditions and flatulated temperature behavior. Moreover, Mokhtari Mehmandoosti et al [27] utilized multi-objective artificial neural network optimization for battery thermal management with pulsating flow, achieving a 27% improvement in maximum temperature and a 50% reduction in maximum temperature difference based on a 2D model. Numerous studies have showcased effective liquid cooling methodologies and channel configurations for battery thermal management, yielding compromised outcomes with respect to the maximum temperatures within the battery pack. However, research regarding the control of battery temperature uniformity and system temperature uniformity, while concurrently reducing the maximum temperature of the battery, remains limited.

In this paper, a novel scanning cooling method for the battery pack is presented. This scanning flow approach employs multiple pipes within the cooling channel, with each inlet valve opening and closing sequentially and cyclically at a specific frequency, resulting in a pulsating flow pattern in each pipe. The study includes a parametric investigation of the cooling performance, exploring variations in the number of pipes, different battery quantities, and scanning frequencies. Additionally, the scanning flow systems are examined and compared with equivalent conventional continuous flow cooling systems having the same battery quantities, contact area, and mass flow rate. Furthermore, experimental analysis is compared with simulation results to validate the thermal management capability of the scanning flow method. This study enhances comprehension of pulsating flow and paves the way for the advancement of scanning flow techniques aimed at enhancing thermal management and achieving temperature uniformity within battery packs and battery surfaces.

II. Problem Definition

The operating temperature significantly affects the charging and discharging performance with regard to voltage window, discharge capacity and life, etc [28]. Operating temperature lower than $20°C$ can lead to significant reduction in power capability, driving range and even freezing of electrolyte. Moreover, operating range higher than $45°C$ can result in battery degradation [29], [30]. The non-uniform, localized high temperature spot can initiate an enhanced Li deposition rate, leading to further battery shorting [31]. Thus, high-power density and fast charging batteries need to consider thermal management to enhance uniform temperature and operate in a suitable temperature range via an efficient cooling system.

This paper proposes a novel scanning flow cooling method for battery thermal management systems. However, the operational mechanism and the influence of parameters on scanning cooling are not yet fully understood. Therefore, this study aims to investigate the effects of scanning cooling and assess its feasibility for battery thermal management.

III. Construction of the Cooling System

The conventional continuous liquid cooling system for batteries has limitations in thermal management due to restricted control overflow states. In contrast, the scanning flow provided independent control for each inlet. Each inlet is programmed to open and close sequentially and cyclically at a certain frequency. Hence, pulsatile flow behavior is applied in each of the pipe. The thermal management characteristics for scanning flow relies on the flow difference between each inlet. Thus, the minimum of two inlets enables the scanning flow characteristics.

Fig 1 (a) presents a ten-pipe 'wrap around' channel design with 12 installed batteries. To simplify the computational complexity of the investigation on parametric study, Fig 1 (b) shows the half model of the same ten-pipe ‘wrap around’ design with two batteries. The geometry construction of the channel and the battery can be defined by eight parameters: the outer radius of the channel R_c, length of the channel L, width at the channel W_c, height of the channel H_c, total length of the inlet L_{ctotal}, the channel wall thickness T_{wall}, pipe number C and the battery number B. The contact area between coolant and the heat resource should be identical in order to reveal the parametric effect for scanning flow cooling efficiency with different inlet numbers. Thus, the length of each pipe can be found by $L_c = \frac{L_{ctotal}}{C}$. Furthermore, the gap thickness between the pipes can be calculated as $T_{gap} = \frac{L - L_{ctotal}}{c+1}$. In certain cases, the T_{gap} may yield infinite values; in such instances, two decimal numbers are retained, and the remaining number is added to the gap thickness at the middle gap of the inlet.

For instance, ten-pipe channel has a gap thickness $T_{gap} = 0.95$ mm, but the middle gap of inlet has a thickness $T_{gap} = 1.00$ mm. Moreover, the length of the battery is identical to the length of the channel L and the radius of the battery can be found by $R_B = R_c - H_c$.

The inlet and battery numbers variation in the following section are presented in 'C_nB_n' format, where 'C_n' stands for the total number of the pipes/inlets and 'B_n' represents the overall number of batteries. For example, Fig 1 (b) demonstrates the cooling system with size C_2B_2, i.e. two battery cells and two pipes/inlets in the system.

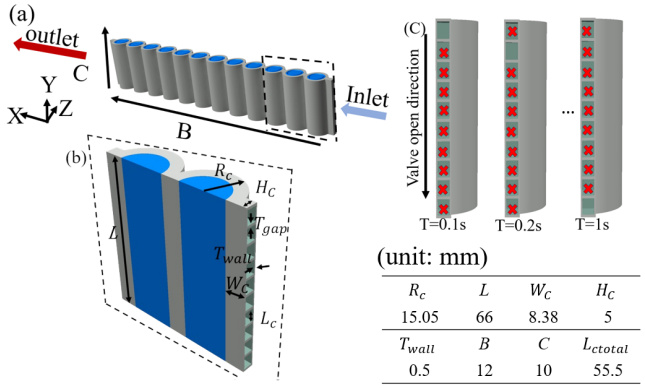

(unit: mm)

R_c	L	W_c	H_c
15.05	66	8.38	5
T_{wall}	B	C	L_{ctotal}
0.5	12	10	55.5

Fig 1 The construction and dimensions of the Wrap around cooling system (a) cooling system with ten pipe and 12 battery cells ($C_{10}B_{12}$), (b) zoomed in half model of ten-pipe and two battery cells system ($C_{10}B_2$), (c) valve opening status with valve switching frequency F=1 Hz for one second.

IV. Numerical Modeling of Scanning Flow Cooling System

The parametric effect on thermal efficiency for scanning cooling encompasses aspects such as inlet opening frequency, the number of inlets, and mass flow rate. These findings are then compared to equivalent conventional continuous flow systems. Fig 2 demonstrates the model of continuous flow and scanning flow. In Fig 2 (a), continuous flow illustrates the flow within a single pipe, inspired by the conventional single cooling pipe approach.

Scanning flow in Fig 2 (b) shows each of the tubes has an independent valve switch on and off the flow. The valve opening order is demonstrated in Fig 2 (c) with an opening frequency F=1Hz for one second of $C_{10}B_2$ cooling system. It demonstrates each valve opens sequentially for 0.1 seconds, with the last valve opening and closing at 1 second. This study investigates the thermal management capability of scanning flow, focusing solely on the cooling tubes for comparison. It is crucial to note that the continuous flow cooling system maintains an identical contact area between the coolant and the heat source, denoted as $L_{ctotal-continous\ flow} = L_{ctotal-scanning\ flow}$.

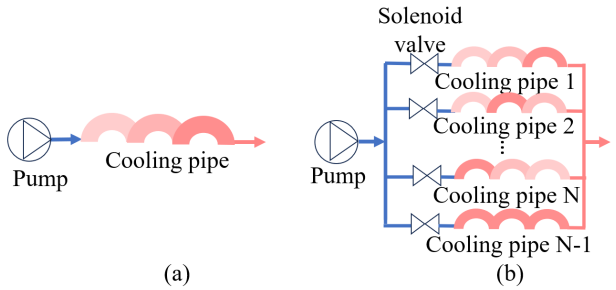

Fig 2 The model for the cooling systems (a) The conventional continuous flow, (b) scanning flow.

The coolant is water with a density $\rho_w = 998.1\ \mathrm{kg/m^3}$, viscosity $\mu = 1.003 \times 10^{-3}\ \mathrm{kg/ms}$ specific heat $c_{pw} = 4182\ \frac{\mathrm{J}}{\mathrm{kg}}/\mathrm{k}$ and thermal conductivity λ_w=0.6 W/m/k. The inlet mass flow rate at the pump is $\dot{m} = 0.0383$ kg / s at 300 K. The channel uses aluminum with a density $\rho_A = 2719\ \mathrm{kg/m^3}$, specific heat $c_{pA} = 871\ \frac{\mathrm{J}}{\mathrm{kg}}/\mathrm{k}$ and thermal conductivity λ_A=202.4 W/m/k. Moreover, the material property of 26650 lithium battery is with thermal conductivity λ_b=3.91 W/m/k specific heat $c_{pb} = 1180\ \frac{\mathrm{J}}{\mathrm{kg}}/\mathrm{k}$ and density $\rho_b = 1760\ \mathrm{kg/m^3}$ [32]. Furthermore, to reduce the computational time, the battery discharge temperature is assumed to be an extreme condition, the temperature rising from 300 K to 330 K within 10 s.

The heat generation of the battery (Q) can be found by:

$$Q = c_{pb} m_b \Delta T\ (\mathrm{J}) \qquad (1)$$

Where m_b presents for the mass of the mass of the battery.

Moreover ΔT is the temperature rise between the initial temperature (T_i) and the final temperature (T_n) of the battery:

$$\Delta T = (T_i - T_n)\ (\mathrm{K}) \qquad (2)$$

The volumetric heat generation q_V by the battery can be obtained:

$$q_V = \frac{Q}{V_b} = c_{pb}\rho_b \Delta T\ (\mathrm{J/m^3}) \qquad (3)$$

Thus, the volumetric heat generation rate of the battery $\dot{q_v}$ can be found and applied as heat generation in CFD:

$$\dot{q_v} = \frac{dQ_V}{dt}\ (\mathrm{W/m^3}) \qquad (4)$$

The inlet velocity can be obtained by Darcy's law:

$$V = \frac{Q_v}{A} = \frac{\dot{m}/\rho_w}{L_c(H_c - 2T_{wall})}\ (\mathrm{m/s}) \qquad (5)$$

Where Q_v is the volume metric flow rate for the water and A is the cross-section area of the pipe.

Furthermore, the flow statues are classified by the Reynold's number (Re) which can be found by:

$$Re = \frac{\mathrm{D}V\rho_w}{\mu} \qquad (6)$$

The diameter of the pipe (D) with a rectangular shape can be calculated by hydraulic diameter equation:

$$D = \frac{2L_c(H_c - 2T_{wall})}{L_c + (H_c - 2T_{wall})}\ (\mathrm{mm}) \qquad (7)$$

The numerical method is used to analyze the thermal management of the cooling systems with different parameters. Simulations are investigated by ANSYS FLUENT 2022R2. Energy conservation equation is opened to calculate the heat exchange. Transient behavior is enabled to allow scanning flow behavior. The turbulence model used for the analysis is $k-\omega$ SST which provides several wall treatment approaches.

Furthermore, other assumptions are taken into consideration in the simulations: 1) the heat generation on the batty is evenly distributed, 2) The battery process has identical thermophysical properties, with no regard for the impact of temperature and state of charge (SOC).

A. Mesh convergency study

A mesh convergence is taken on scanning flow model and equivalent continuous models are presented in Fig 3. The maximum temperature is selected due to its significance as one of the most crucial parameters for the study. The with a maximum element size 0.5mm to ensure accurate mesh quality. A prism layer mesh with a growth rate of 1.2 is used to specify the flow near the wall inside of the pipe. The mesh setting with mesh element numbers 608765 and 898347 are selected for scanning flow model and equivalent continuous models, respectively.

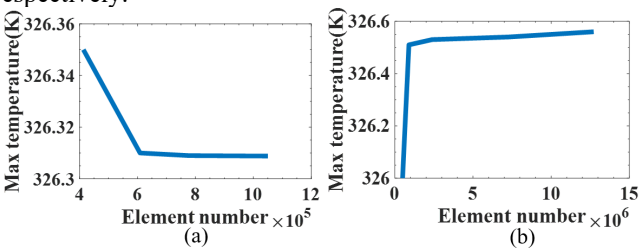

Fig 3 Mesh convergence study (a) Scanning flow cooling system C_2B_2 with valve switching frequency 0.25Hz. (b) equivalent continuous cooling with two batteries.

B. Time step independency study

The time step can highly impact the temperature results for scanning cooling as it requires frequency valve charging to enhance the cooling effect. Thus, the time step independence study reveals the minimum time step that is required to get accurate results. It is noticed that each valve opening time requires a different time step, and the time step size reduces as the frequency increases. Thus, Fig 4 demonstrates the time step independency study for C_2B_2 with valve switching frequency F=2 Hz. The results show the time step homogenized at $\Delta t = 0.1$ s.

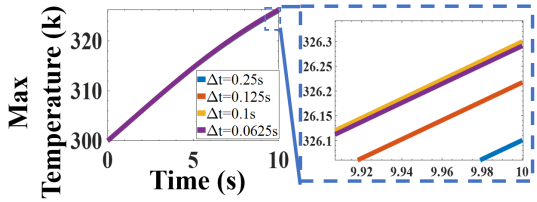

Fig 4 Time step independency study.

V. Parametric Study of Scanning Flow

The parametric study demonstrates the parametric effect on the scanning flow cooling efficiency. Three variables are considered charging in this study for scanning flow and equivalent continuous flow: the battery number *B*; the pipe number *C*; and the valve switch frequency *F*. The battery numbers of two, six, and twelve are chosen to comprehensively assess the performance of the cooling system under varying load conditions and scaling effects. The inlet mass flow rate remains constant, and the profile of the channel geometry is fixed. The maximum, minimum, average and the difference of the temperatures on the batteries are recorded and compared. Furthermore, scanning flow is compared with equivalent continuous flow to better understand its thermal management capabilities.

A. Two battery cooling system

Cooling systems C_2B_2, $C_{10}B_2$ and $C_{20}B_2$ with valve switching frequencies 0.25 Hz, 0.5 Hz, 1 Hz and 2 Hz are studied and compared to an equivalent one-pipe continuous flow cooling system with two batteries. Fig 5 demonstrates the thermal behaviors of the batteries in the two-battery (B_2) cooling systems with scanning flow at different frequencies and continuous flow as a function of time. Fig 5 (a) presents the non-linear increasing trends for all cooling systems, illustrating that the maximum temperature increases with time. The maximum temperature happened on the core of the batteries where it has the largest distance from the cooling channel. The largest value is for C_2B_2 0.25 Hz with a value of 326.3 K, which is 0.2 K smaller than continuous flow with a value of 326.5 K. The lowest maximum temperature is for $C_{20}B_2$ 2 Hz with a value of 325.7 K, which is 1.2 K smaller than continuous flow. Moreover, the difference for the maximum temperature values between 10-pipe and 20-pipe at identical frequencies are very similar, with a maximum difference of 0.04% at 2 Hz.

Fig 5 (b) demonstrates non-linear increasing trends for all cooling systems with scanning and continuous flow. The oscillation trends for the scanning flow are caused by the valve switching leading to the fluid mass flow rate change. The minimum temperature happened on the surfaces of the batteries where they are directly in contact with the cooling channel. The largest minimum temperature is C_2B_2 0.25 Hz at 10 s with a value of 304.4 K, which is 0.5 K higher than continuous flow at the same time. The smallest minimum temperature at 10 s is $C_{20}B_2$ 2 Hz with a value of 303 K, which is 0.9 K smaller than continuous flow. Similarly, the difference in the battery minimum temperature between 10-pipe and 20-pipe cooling systems is very similar, with a maximum difference 0.2 K measured at 1 Hz. It is noticed in 10-pipe and 20-pipe cooling channel, that the minimum temperature decreases with the valve switching frequency increases with the identical pipes numbers. However, the frequency effect for 2-pipe cooling channel seems more random due to the lack of channel numbers that lead to the velocity change caused by the switching valve process having a larger influence on the minimum temperature.

Fig 5 (c) demonstrates the average temperature for all batteries in the system. The nonlinear positive trends for all cooling systems show the average temperature smoothly increases with time increases. The maximum average temperature is at C_2B_2 0.25 Hz with a value of 316.7 K which is 0.2 K smaller than continuous flow with a value of 316.9 K. $C_{20}B_2$ 1 Hz has the lowest average temperature with a value of 315.1K at 10s, which is 1.8 K lower than continuous flow. Moreover, the temperature rising (ΔT)with channel $C_{20}B_2$ 1 Hz is 49.7% reduced compared to the battery temperature rising without cooling.

The average temperature difference illustrates the temperature uniformity and is presented in Fig 5 (d). Unlike other thermal behaviors, the trends for different pipe numbers

and frequencies vary. The decreasing trend for C_2B_2 1Hz, $C_{10}B_2$ and $C_{20}B_2$ illustrate the average temperature at the battery next to the inlet is lower than the battery close to the outlet. This is because the inlet water temperature is cooler than outlet temperature. However, it is noticed for C_2B_2 and continuous flow has a positive trend due to the corrugated channel shape generating vertex between the 'arch' shapes and reduced the local flow speed and increased the water temperature. C_2B_2 0.5 Hz has the maximum average temperature difference with a value of 0.059 K, which is 33.7% lower than continuous flow. The minimum average temperature difference is at C_2B_2 2 Hz with a value of 0.007 K at 10 s, which is 92% smaller than the continuous flow with a value of 0.089 K.

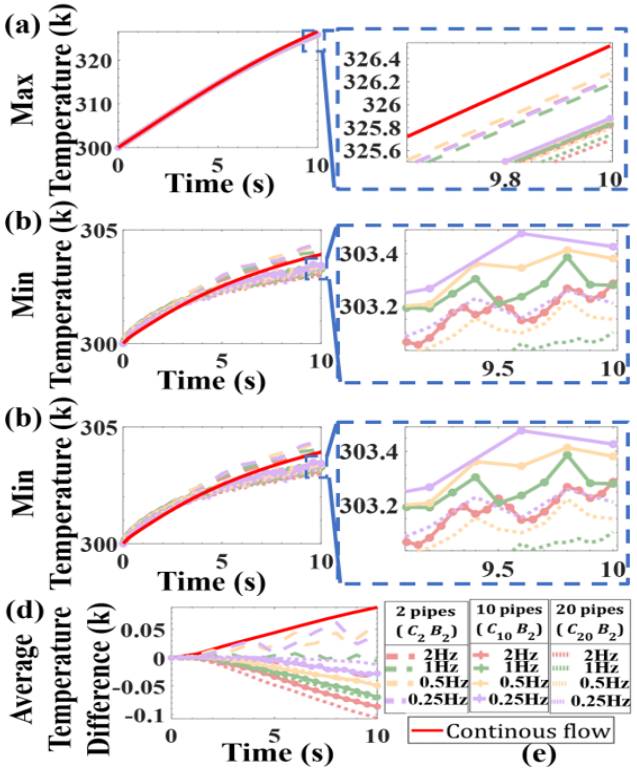

Fig 5 Battery temperatures as a function of time for two battery cooling system with continuous and scanning flow. (a) maximum temperature (b) minimum temperature, (c) average temperature, (d) average temperature difference.

B. Six battery cooling system

Six battery cooling systems for scanning flow including: C_2B_6, $C_{10}B_6$ and $C_{20}B_6$ with valve switching frequencies 0.25 Hz, 0.5 Hz, 1 Hz and 2 Hz are studied and compared to an equivalent one-pipe continuous flow cooling system with six batteries. Fig 6 (a) demonstrates the non-linear increasing trends for all cooling systems, and the scanning flow has a lower maximum temperature than the continuous flow. The smallest magnitude of the maximum temperature at 10 s is at $C_{20}B_6$ 2 Hz with a value of 325.84 K, which is 0.675 K smaller than continuous flow. Moreover, the maximum temperature for $C_{10}B_6$ at different valve switching frequencies are all most identical. The largest difference is between 2 H and 0.25 Hz with a value of 0.01 K.

Fig 6 (b) presents the non-linear increasing trends for all cooling systems, and the scanning flow has a lower minimum temperature value than continuous flow. Oscillation trends for the scanning flow caused by switching valves led to a short time temperature increase. The smallest magnitude of the minimum temperature at 10 s is at $C_{20}B_6$ 2 Hz with a value of 302.97 K, which is 2.25 K smaller than continuous flow. C_2B_6 0.25 Hz has the largest minimum temperature which is 1.66 K higher than $C_{20}B_6$ 2 Hz and 0.59 K smaller than continuous flow. Moreover, the trend for 0.25 Hz in two and six battery systems is very similar. The cooling system with identical pipe numbers at 2 Hz frequency has the lowest minimum temperature before 4 s, then it gradually increases to the highest minimum temperature. This behavior is caused by the battery temperature instantly increasing while the fluid velocity decreases during valve charging, and the flow is unable to transfer all the excessive heat. The difference in the battery minimum temperature between 10-pipe and 20-pipe cooling systems is very similar, as demonstrated in a zoomed purple box, with a maximum difference 0.3 K measured at 1 Hz.

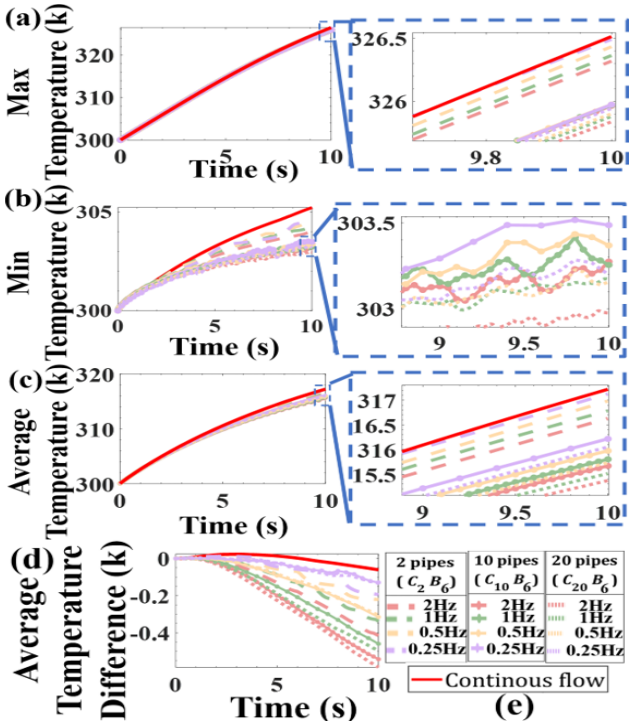

Fig 6 Battery temperatures as a function of time for six battery cooling system with continuous and scanning flow. (a) maximum temperature (b) minimum temperature, (c) average temperature, (d) average temperature difference.

The average temperature of all batteries in the system is presented in Fig 6 (c), demonstrating the scanning flow as a lower battery average temperature than the continuous flow. C_2B_6 0.25 Hz has the maximum average temperature with a value of 317.13 K, which is 0.1 K smaller than continuous flow. Moreover, $C_{20}B_6$ 1 Hz has the lowest average temperature with a value of 315.36 K at 10 s, which is 1.86 K lower than continuous flow. Moreover, the temperature rising (ΔT)with channel $C_{20}B_6$ 1 Hz is 48% reduced compared to the battery temperature rising without cooling.

Fig 6 (d) shows decreasing trends for all cooling systems. The minimum average temperature difference for scanning flow is at $_{10}B_{6}$ 0.25 Hz and $C_{20}B_{6}$ 0.25 Hz with a value of -0.135 K, that is 2.2 times larger than the continuous flow. Furthermore, the largest average temperature difference is at $C_{20}B_{6}$ 2Hz, that is 9.6 times larger than continuous flow. However, all average temperature difference values for the scanning flow are smaller than 0.6 K. It is noticed for all scanning flow system, the lower the valve switching frequency the lower the average temperature difference.

C. Twelve battery cooling system

Three cooling systems: C_2B_{12}, $C_{10}B_{12}$ and $C_{20}B_{12}$ are selected for investigating the thermal behaviour of twelve battery cooling systems with valve switching frequencies 0.25 Hz, 0.5 Hz, 1 Hz and 2 Hz. The nonlinear increasing trends of maximum temperature for all cooling systems are presented in Fig 7. The results demonstrate the scanning flow has a lower maximum temperature compared to continuous flow in twelve battery system with a maximum difference 1.15 K. Similar to cooling systems with six battery numbers, the maximum temperature decreases with frequency increases. Furthermore, the distance between the trends is decreasing with pipe number increases indicating the pipe number effect on maximum temperature is decreasing.

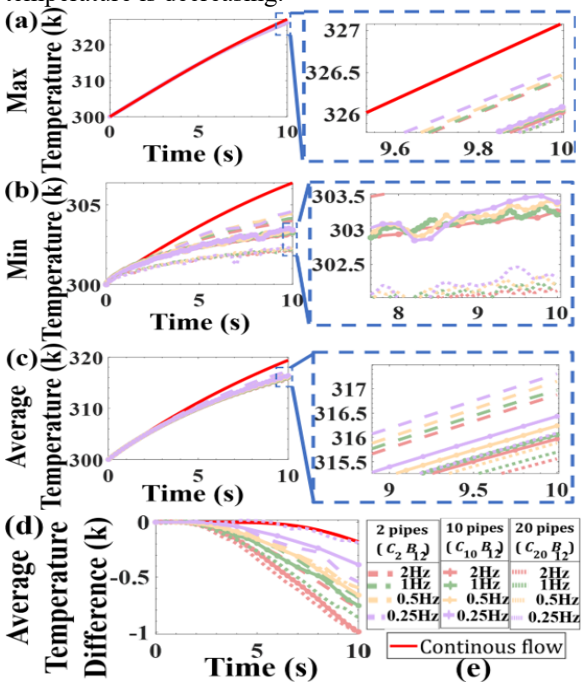

Fig 7 12 Battery temperatures as a function of time for six battery cooling system with continuous and scanning flow. (a) maximum temperature (b) minimum temperature, (c) average temperature, (d) average temperature difference.

Fig 7 (b) shows both scanning and continuous flow have increasing trends for minimum temperature in the cooling system. The lowest minimum temperature is $C_{20}B_{12}$ 2 Hz with 302.11 K, that is 4.25 K smaller than continuous flow. Moreover, the largest minimum temperature for scanning flow is $C_{20}B_{12}$ 0.25 Hz with a value 304.58 K, that is 1.78K. Unlike two and six battery system, the minimum temperature between 10-pipe and 20-pipe are very different with a maximum difference 1.1 K at 2 Hz and 0.25 Hz.

The average temperature of the batteries is presented in Fig 7 (c) with nonlinear increasing trend for both scanning and continuous flow. The results show the scanning flow has a lower average temperature than continuous flow. The minimum average temperature is 315.56 K at $C_{20}B_{12}$ 2 Hz, that is 3.84 K smaller than continuous flow. Furthermore, the temperature rising (ΔT) with channel $C_{20}B_{6}$ 2 Hz is 48.13% reduced compared to the battery temperature rising without cooling.

The average temperature difference presents in Fig 7 (d) demonstrates it decreases with time increases. The continuous flow has the minimum temperature difference, however, the scanning flow $C_{20}B_{12}$ 0.25 Hz is only 6.7% higher than continuous flow. Furthermore, the largest average temperature difference is at $C_{20}B_{10}$ 2 Hz, that is 5.6 times larger than continuous flow. However, all average temperature difference values for the scanning flow are lower than 1 K. Similar to six battery cooling system, the lower valve switching frequency the lower average temperature difference.

D. Discussion

The parametric study demonstrates the scanning flow has a better cooling effect for maximum, minimum and average battery temperatures than continuous flow when the battery number in the cooling system is larger than two. This is attributed to the pulsatile flow generated within the scanning cooling pipe, facilitating the mixing of water to lower its temperature. The results also demonstrate the larger numbers of batteries in the system, the better the cooling effect of scanning flow is compared to continuous flow.

Increasing the number of pipes can minimize the maximum, minimum, average temperature, and average temperature difference for all battery configurations with the same valve switching frequency. As the number of pipes increases, the cross-sectional area of the pipes decreases, resulting in an increase in flow velocity that enhances the cooling effect.

Furthermore, for maximum, minimum and average battery temperatures, the cooling effect can be improved by increasing the valve switch frequency. This adjustment is attributed to alterations in water supply frequency and flow patterns within the pipe. The optimization of valve switching frequency is necessary to minimize the average temperature difference across the system. The valve switching frequency exerts a more significant influence on the minimum average temperature difference than the number of pipes in both six and twelve battery configurations. Notably, in a two-battery system, the effects of both factors appear to be relatively similar. The scanning flow method offers increased controllability compared to continuous flow over cooling processes, as it facilitates adaptive valve switching frequencies. However, fitting a mechanical valve to each channel would pose significant challenges in achieving compactness.

VI. Fluid Behavior Analysis

The phenomenon in parametric study for battery temperatures can be explained by fluid mechanisms. The fluid behavior

analysis includes the heat distribution and the velocity behaviors to explore the flow characteristics that can enhance the cooling efficiency. The scanning flow shows an enhanced cooling efficiency than continuous flow in a cooling system with large numbers of the batteries. Thus, $C_{20}B_{12}$ 2 Hz cooling system is selected to study the fluid behavior and compare with equivalent continuous flow cooling system.

Fig 8 (a) demonstrates the thermal behavior in observed results shown in Section V. The temperature for the cooling pipes has a significant increment from inlet to outlet with a temperature range from 300 K to approximately 311 K. Furthermore, the highest temperatures for the channel are located between batteries similar to the heat distribution highlighted by red box. Unlike scanning flow, continuous flow has huge temperature unevenness for the batteries. Overall, the temperature distribution for each of the battery surfaces has lower temperature at both ends with a value of 303 K and higher temperatures at the middle with a value of approximately 311.2 K of the cylinder due to the pipe location and the thickness at the sides of the pipe. Hence the temperature difference on the battery surface is 8.2 K.

Fig 8 (b) demonstrates the heat distribution of scanning flow cooling system $C_{20}B_{12}$ 2 Hz. The temperature for the cooling channel is gradually increased from inlet to outlet with a temperature range from 300 K to approximately 303 K. Furthermore, the temperature for the pipes is evenly distributed without any local heating spot. The temperature on the battery surfaces is very even, the maximum temperature difference on the battery surface is 3 K which is 62.5% improved compared to continuous flow.

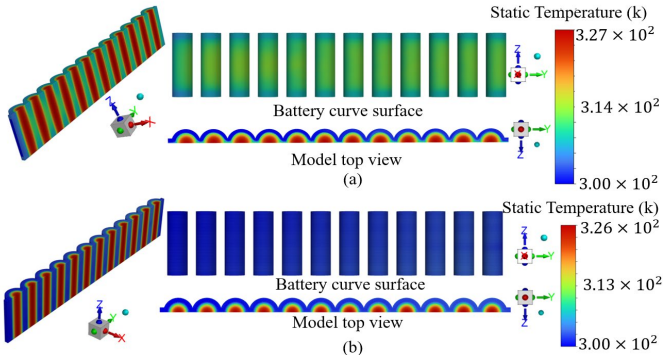

Fig 8 Heat distribution of cooling system (a)equivalent continuous flow cooling, (b) system scanning flow cooling system $C_{20}B_{12}$ 2 Hz.

Flow mechanics for scanning and equivalent continuous flow at 10s demonstrated in Fig 9 reveals the heat distribution and the thermal behavior of the cooling systems. Fig 9 (a) demonstrates the flow mechanics of an equivalent continuous flow cooling system at 10 s. The maximum speed location for the continuous flow is located near the connection of each arch with a value of 0.088 m/s. Low-velocity regions formed into vortex shapes with the largest detached flow layer thickness around 2.5 mm that are highlighted by blue and orange boxes. Furthermore, low velocity flow detached from the wall with maximum 1mm thickness can be seen near the bottom arch walls. The flow inside of the pipe reaches a steady state and the low-velocity regions stays at the same place and are heated up generating hotspots. Hence temperature un-uniformity on the battery surface is found as demonstrated in Fig 8 (a).

Fig 9 (b) presents the flow mechanics of the scanning flow cooling system at 10s for all pipes. The valve for pipe-20 is just closed, while pipe-1 opens simultaneously. Nonetheless, pipes 2, and 3 continue to exhibit distinct flow velocities and flow mechanisms. Pipe-20 registers the highest velocity, reaching a value of 6.48 m/s, which is approximately 77 times greater than that observed in continuous flow. This disparity can be attributed to the smaller cross-sectional area of each pipe, as explained by Darcy's law in (5). While a high Reynolds number in continuous flow increases the boundary layer thickness, it is important to note that pulsating flow can disrupt the boundary layers that form along solid boundaries [22]. Furthermore, the low speed flow layer at the bottom of the arch is approximately 0.25mm, which is four times smaller than the equivalent conventional continuous model. Therefore, based on the Reynolds analogy the heat transfer should increase in such conditions[33]. Vortex path lines highlighted by purple box are at the first half of each arch that is created by pipe geometry and the velocity is enhanced by scanning flow behavior. Furthermore, a low-speed flow, ranging from 0 m/s to 0.88 m/s, is discernible at the junctures of each arch, attributable to the influence of pipe geometry. This phenomenon may induce localized temperature elevation. Notably, the velocity magnitude observed is nearly ten times greater than the maximum speed of an equivalent continuous flow model, strategically implemented to enhance heat exchange efficiency.

Valve for pipe-1 allows all flows to enter with an inlet velocity of 3.46 m/s and a Reynolds number of 1.134×10^4, it indicates that the inlet flow is turbulent. The highest speed in all pipes is acting in Pipe-1 with a velocity 8.86 m/s, almost 100 times larger than the equivalent conventional continuous model.

The high-speed turbulence is predominantly concentrated around the first two arches near the inlet, resulting from the relatively short valve opening time. The fluid path line at these arches, illustrated in the green box, shows the formation of swirl flow. Additionally, the high-speed swirl flows and vortices near the pipe wall minimize boundary layer thickness, measured at approximately 0.35 mm. Turbulence with maximum velocity is observed in the first half of the arch due to geometric factors. While most regions exhibit relatively low-speed blue-green colors, their velocities are maintained at approximately 2.2 m/s, which is notably 24 times greater than the maximum velocity in the equivalent continuous flow model.

The vortex and swirl flows within the pipe possess angular momentum, enhancing water mixing and reducing the boundary layer thickness to improve heat exchange[34]. Additionally, these vortex and swirl flows may induce boundary layer separation, thereby influencing the boundary layer thickness. Furthermore, the pulsating flow behavior contributes to the continuous generation of vortices and swirl flows, sustaining high heat transfer efficiency [35].

The sequential opening and closing of valves in the scanning flow method significantly alter the flow speed and fluid dynamics within all pipes, effectively mitigating hotspots. This process is evidenced by substantial variations in both the maximum speed magnitude and its location within the pipes.

The scanning flow ensures that water flows into one pipe at a time, maximizing the velocity within that pipe. Consequently, the flow undergoes significant speed fluctuations, fostering boundary layer removal, increasing turbulence, and eliminating low-velocity regions. This dynamic process contributes to the overall reduction of hotspots.

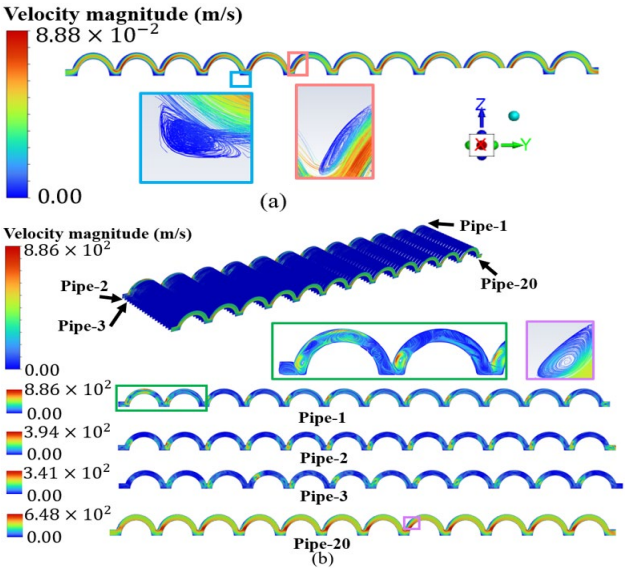

Fig 9 Flow behavior for the cooling systems at 10s, (a) continuous flow cooling system, (b) scanning flow cooling system $C_{20}B_{12}$ 2 Hz.

VII. Experiment analysis

A. Manufacturing and materials

A complete cooling channel with inlet and outlet nozzles was manufactured using stereolithography (SLA) resin 3D printing technology to minimize excessive internal support structures and enhance sealing capability. However, several leakage issues were encountered, necessitating an intricate coating procedure with the same resin material. Additionally, the model requires thorough curing using a UV curing station for two minutes, followed by at least two days of exposure to natural sunlight. This extended curing process is essential due to the model's complex geometry and size.

The main limitation lies in achieving and maintaining a minimal wall thickness to enhance heat transfer, given its very low thermal conductivity. Considering all these limitations including the manufacturing bedding size and installation tolerance for pipes, a test sample C_3B_4 is manufactured with modified dimensions presented in Appendix.

The chemical reactions occurring during battery charging/discharging pose potential dangers. To address safety concerns, cartridge heaters are utilized as substitutes for batteries to simulate heat generation. Four stainless steel-coated cartridge heaters, each with a diameter of 6 mm, length of 80 mm, voltage of 24 V, and a maximum power output of 50W, are employed to generate heat. Furthermore, the material properties of resin and cartridge heater are listed in Table I.

Table I
MATERIAL PROPERTIES OF RESIN AND CARTRIDGE HEATER

	Resin	Cartridge heater
Density ρ (kg/m^3)	1246.6	7749.8
Heat capacity Cp (J/(kg K))	1160.6	487.52
Thermal conductivity λ (W/(m K))	0.188	14.618

B. Cooling experiment

The cooling capability of the scanning flow method is assessed through experiments, demonstrating its feasibility for battery thermal management. The cooling experiment is repeated five times, with intervals of at least four hours between each repetition to ensure independent results.

The experimental setup and apparatus for cooling experiment are presented in Fig 10. The Flojet RLF diaphragm pump is employed to transfer water into the cooling system from the water tank, maintaining a constant flow rate of 0.0068 kg/s, which is monitored by a flow speed sensor. A resin flow separation part is installed between the water pump and solenoid valves to distribute one flow to each solenoid valve. Thus, the maximum speed at the pump is limited by the water pressure inside the resin flow separation part. Six solenoid valves that create a scanning flow effect with 1 Hz valve switching frequency are connected to each channel inlet nozzle with transparent pipes. The arrangement of this valve switching frequency configuration not only achieves an effective cooling effect but also enables convenient observation and monitoring of the waterflow throughout the scanning flow process. An independent valve controlling system controls solenoid valves to achieve various valve switching frequencies.

Four cartridge heaters, each delivering a power output of 0.98 W, are employed to gradually raise the temperature of the channel over a duration of 600 seconds. The constrained power output prevents channel melting and promotes improved heat transfer, addressing the low thermal conductivity of the resin. Four thermocouples stick on the middle of the cartridge heater surface to monitor the heat change. The temperature data is collected by the temperature data logger with a data recording frequency 0.5 Hz. The gap between cartridge heaters and the channel is fulfilled by thermal paste to improve the thermal conductivity. Furthermore, the connections between resin nozzle and pipe with relatively low water pressure should be fastened using plastic zip tie instead to avoid overstressing the model. Radiator is connected with channel outlet nozzles with pipes to cool down the coolant before entering the water tank. Moreover, thermocouples are placed in the water tank and next to the setups to monitor the water temperature and ambient temperature with values of 293.5 K and 295.5 K, respectively.

The limitations of the current experiment prevent the measurement of temperature uniformity across the cartridge heaters and their surfaces. These limitations stem from the slight variations in power output among the cartridge heaters, attributed to circuit resistance and losses. Additionally, the small surface areas of the cartridge heaters constrain the placement of multiple thermocouples.

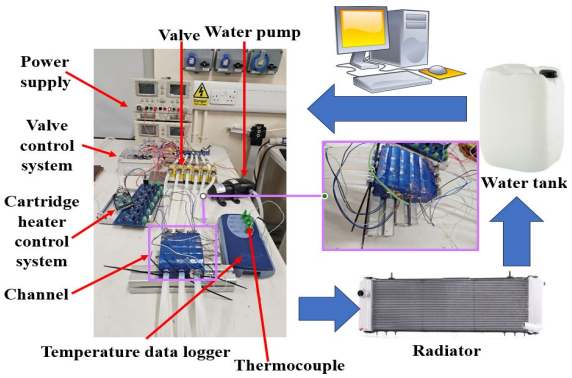

Fig 10 Experimental setup.

C. Results and validation

The cooling experiment validation study between the experiment and computational model demonstrates the reliability of computational models. The material properties listed in Table I are used for numerical analysis in Ansys Fluent. Mesh Convergence studies are performed with a total element of 7765731 for discretization. The average temperature on each cartridge heater is collected in simulation for validation. Furthermore, the actual power output from the cartridge heaters is measured at 0.799W and implemented in simulation.

Fig 11 shows the overall average temperature of the cartridge heater as a function of time. The average temperature trends between experimental results and simulation results are similar. The simulation result for scanning flow presents the temperature increases from 295.5 K to a maximum temperature 298 K at 131 s, then starts to stabilize. The experimental results show a maximum temperature of 298.3 K at 298.5 s. The experimental results for continuous flow indicate that the maximum temperature, 299.5 K, occurs between 360 s to 600 s, which is 1.2K smaller than the maximum temperature for scanning flow. However, the maximum error rate between experimental and numerical results are 0.17% at 48.48 s for scanning flow and 0.27% at 80s for continuous flow, respectively. It is important to emphasize that the valve switching frequency of the scanning flow in the experiment was not optimized for superior performance in reducing maximum temperatures.

The scanning flow method exhibits exceptional cooling capabilities. The average temperature under natural convection, as determined experimentally, is illustrated in Fig 11. At 600 s, the maximum temperature peaks at 321.9 K, demonstrating a 23 K reduction compared to scanning flow cooling.

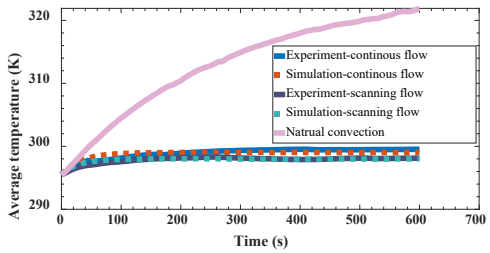

Fig 11 Experimental and simulation results of average temperature on cartridge heater as a function of time.

VII. Conclusion

This study introduces an innovative microchannel cooling system incorporating a scanning flow approach for vehicular battery thermal management. A substantial number of CFD simulations, conducted with a refined mesh, were executed on high-performance computing clusters. These simulations encompassed various valve switching frequencies, pipe configurations, and battery quantities, with the overarching aim of elucidating the thermal dynamics of the system.

Parametric study was undertaken to assess the effects of battery quantity, valve switching frequency, and pipe configuration on cooling efficiency. Findings from this investigation demonstrate the superiority of the scanning flow method over continuous flow in regulating maximum, minimum, and average battery temperatures, particularly evident with more than two batteries in the cooling system. Furthermore, an in-depth analysis of fluid behavior provided insights into temperature distribution and flow dynamics, indicating lower and more uniform temperatures across the batteries in scanning flow cooling systems. The maximum average temperature difference has been reduced by 92%, representing a significant improvement compared to the works of Mokhtari Mehmandoosti et al [27] and Xu et al. [12], which reported improvements of 42% and 84.51%, respectively. The temperature evenness on the battery surface improved 62.5% compared to equivalent continuous flow.

Fluid mechanics analysis demonstrated that scanning flow exhibits pulsating behavior, diminishing boundary layer thickness and dynamically altering pipe flow to augment cooling. Additionally, valve switching in scanning flow leads to notably higher flow velocity compared to continuous flow, consequently enhancing turbulence.

Finally, cooling experiments were conducted using an SLA 3D printed channel and stainless-steel cartridge heaters as battery substitutes. The excellent correlation, with a maximum error rate of 0.17%, between experimental and simulation results for scanning cooling underscores the reliability of the numerical models. Fu

The results of this study can provide useful reference for flow control in liquid cooling systems to provide superior battery temperature uniformity and minimize the cell temperature. In addition, this scanning flow method is beneficial for the future fast charging battery with high energy density to control the temperature in a short time. Furthermore, the results suggested an AI controlled real-time battery thermal analysis to optimize[36], [37] valve switching frequency can be studied to adapt to the battery needs. Furthermore, a large number of battery matrices need to be further studied.

APPENDIX

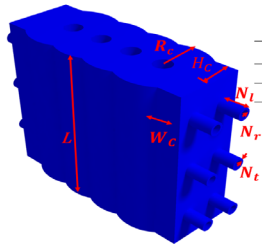

Channel parameters

R_c	L	W_C	H_C	T_{wall}	L_{ctotal}
19	80	10.7	15	0.5	75.9

(mm)

Nozzle parameters

N_l	N_r	N_t
10	3	1

(mm)

Fig 12 Dimension of the 3D printing cooling channel used in the experiment.

REFERENCES

[1] H. Tu, H. Feng, S. Srdic, and S. Lukic, "Extreme Fast Charging of Electric Vehicles: A Technology Overview," *IEEE Trans. Transp. Electrif.*, vol. 5, no. 4, pp. 861–878, Dec. 2019.

[2] Y. Liu, Y. Zhu, and Y. Cui, "Challenges and opportunities towards fast-charging battery materials," *Nat. Energy*, vol. 4, no. 7, pp. 540–550, Jun. 2019.

[3] J. Jaguemont, M. Abdel-Monem, N. Omar, J. van Mierlo, and P. van den Bossche, "Thermal Effect of Fast-Charging Profiles on Lithium-Ion Batteries," in *2018 21st International Conference on Electrical Machines and Systems (ICEMS)*, 2018, pp. 2127–2132.

[4] N. H. F. Ismail, S. F. Toha, N. A. M. Azubir, N. H. Md Ishak, M. K. Hassan, and B. S. KSM Ibrahim, "Simplified Heat Generation Model for Lithium ion battery used in Electric Vehicle," *IOP Conf. Ser. Mater. Sci. Eng.*, vol. 53, p. 012014, Dec. 2013.

[5] G. Zhao, X. Wang, and M. Negnevitsky, "Connecting battery technologies for electric vehicles from battery materials to management," *iScience*, vol. 25, no. 2, p. 103744, Feb. 2022.

[6] A. Pesaran, "Battery Thermal Management in EVs and HEVs : Issues and Solutions," *Adv. Automot. Batter. Conf.*, no. January 2001, p. 10, 2001.

[7] P. Tirkey, R. K. Pandey, S. Kumar, and J. N. Mahto, "A Detailed Review on Battery Cooling Systems for Electric Vehicles," *Proc. 2022 1st IEEE Int. Conf. Ind. Electron. Dev. Appl. ICIDeA 2022*, pp. 45–50, 2022.

[8] N. Farouk, A. A. Alotaibi, A. H. Alshahri, and K. H. Almitani, "Challenges in incorporating phase change materials into thermal control units for lithium-ion battery cooling," *J. Energy Storage*, vol. 49, p. 104094, May 2022.

[9] D. Zhao and G. Tan, "A review of thermoelectric cooling: Materials, modeling and applications," *Appl. Therm. Eng.*, vol. 66, no. 1–2, pp. 15–24, May 2014.

[10] Z. Guo, J. Xu, Z. Xu, M. Mubashir, H. Wang, and X. Mei, "A Lightweight Multichannel Direct Contact Liquid-Cooling System and Its Optimization for Lithium-Ion Batteries," *IEEE Trans. Transp. Electrif.*, vol. 8, no. 2, pp. 2334–2345, Jun. 2022.

[11] J.-W. Han, K. S. Garud, E.-H. Kang, and M.-Y. Lee, "Numerical Study on Heat Transfer Characteristics of Dielectric Fluid Immersion Cooling with Fin Structures for Lithium-Ion Batteries," *Symmetry (Basel).*, vol. 15, no. 1, p. 92, Dec. 2022.

[12] H. Xu, X. Zhang, G. Xiang, and H. Li, "Optimization of liquid cooling and heat dissipation system of lithium-ion battery packs of automobile," *Case Stud. Therm. Eng.*, vol. 26, p. 101012, Aug. 2021.

[13] Q. Ye, Y. Zhang, and J. Wei, "A comprehensive review of pulsating flow on heat transfer enhancement," *Appl. Therm. Eng.*, vol. 196, p. 117275, Sep. 2021.

[14] B. Yuan, Y. Zhang, L. Liu, J. Wei, and Y. Yang, "Experimental research on heat transfer enhancement and associated bubble characteristics under high-frequency reciprocating flow," *Int. J. Heat Mass Transf.*, vol. 146, p. 118825, Jan. 2020.

[15] M. Hemmat Esfe, M. Bahiraei, A. Torabi, and M. Valadkhani, "A critical review on pulsating flow in conventional fluids and nanofluids: Thermo-hydraulic characteristics," *Int. Commun. Heat Mass Transf.*, vol. 120, p. 104859, Jan. 2021.

[16] S. Candel, "Combustion dynamics and control: Progress and challenges," *Proc. Combust. Inst.*, vol. 29, no. 1, pp. 1–28, Jan. 2002.

[17] M. Dietrich, L. W. Yang, and G. Thummes, "High-power Stirling-type pulse tube cryocooler: Observation and reduction of regenerator temperature-inhomogeneities," *Cryogenics (Guildf).*, vol. 47, no. 5–6, pp. 306–314, May 2007.

[18] R. K. Shah, M. R. Heikal, B. Thonon, and P. Tochon, "Progress in the numerical analysis of compact heat exchanger surfaces," 2001, pp. 363–I.

[19] H. Xian, D. Liu, F. Shang, Y. Yang, and G. Chen, "Experimental Study on the Heat Transfer Enhancement of Oscillating-Flow Heat Pipe by Acoustic Cavitation," *Dry. Technol.*, vol. 27, no. 4, pp. 542–547, Mar. 2009.

[20] M. Shu, D. Qing, and H. Wang, "Study on Heat Transfer Performance of Pulsating Flow in Convergent-Divergent Tube," *IOP Conf. Ser. Earth Environ. Sci.*, vol. 153, p. 032023, May 2018.

[21] P. K. Papadopoulos and A. P. Vouros, "Pulsating turbulent pipe flow in the current dominated regime at high and very-high frequencies," *Int. J. Heat Fluid Flow*, vol. 58, pp. 54–67, Apr. 2016.

[22] Y. Wang, Y.-L. He, W.-W. Yang, and Z.-D. Cheng, "Numerical analysis of flow resistance and heat transfer in a channel with delta winglets under laminar pulsating flow," *Int. J. Heat Mass Transf.*, vol. 82, pp. 51–65, Mar. 2015.

[23] J. Tang and P. Luk, "Wearable Bio-Inspired Pulsating-Flow Cooling for Live Garments Based on a Novel Design of Ferrofluid Micro-Valve," *Energies*, vol. 15, no. 23, p. 8826, Nov. 2022.

[24] J. Tang and P. C. K. Luk, "Ferrofluid-Based Shape-Controllable and Fast-Responsive Micro-Pumping and Valving Actuation," in *2022 IEEE International Instrumentation and Measurement Technology Conference (I2MTC)*, 2022, pp. 1–6.

[25] P. C. K. Luk and J. Tang, "Wearable Bio-Inspired Pulsating Flow Cooling for Live Garments," in *2022 IEEE International Instrumentation and Measurement Technology Conference (I2MTC)*, 2022, pp. 1–6.

[26] D. Li, W. Zuo, Q. Li, G. Zhang, K. Zhou, and J. E, "Effects of pulsating flow on the performance of multi-channel cold plate for thermal management of lithium-ion battery pack," *Energy*, vol. 273, p. 127250, Jun. 2023.

[27] M. Mokhtari Mehmandoosti and F. Kowsary, "Artificial neural network-based multi-objective optimization of cooling of lithium-ion batteries used in electric vehicles utilizing pulsating coolant flow," *Appl. Therm. Eng.*, vol. 219, p. 119385, Jan. 2023.

[28] S. Panchal, I. Dincer, M. Agelin-Chaab, M. Fowler, and R. Fraser, "Uneven temperature and voltage distributions due to rapid discharge rates and different boundary conditions for series-connected LiFePO 4 batteries," *Int. Commun. Heat Mass Transf.*, vol. 81, pp. 210–217, Feb. 2017.

[29] J. Wang *et al.*, "Cycle-life model for graphite-LiFePO4 cells," *J. Power Sources*, vol. 196, no. 8, pp. 3942–3948, Apr. 2011.

[30] N. Yang, X. Zhang, B. Shang, and G. Li, "Unbalanced discharging and aging due to temperature differences among the cells in a lithium-ion battery pack with parallel combination," *J. Power Sources*, vol. 306, pp. 733–741, Feb. 2016.

[31] Y. Zhu *et al.*, "Fast lithium growth and short circuit induced by localized-temperature hotspots in lithium batteries," *Nat. Commun.*, vol. 10, no. 1, p. 2067, May 2019.

[32] Z. An, C. Zhang, Y. Luo, and J. Zhang, "Cooling and preheating behavior of compact power Lithium-ion battery thermal management system," *Appl. Therm. Eng.*, vol. 226, no. 66, p. 120238, 2023.

[33] H. A. HAVEMANN and N. N. N. RAO, "Heat Transfer in Pulsating Flow," *Nature*, vol. 174, no. 4418, pp. 41–41, Jul. 1954.

[34] P. Novotny, B. Weigand, F. Marsik, C. Biegger, and M. Tomas, "Flow structures in a swirl flow - vortex breakdown condition," *J. Phys. Conf. Ser.*, vol. 1045, p. 012031, Jun. 2018.

[35] K. A. Ibrahim, P. Luk, and Z. Luo, "Cooling of Concentrated Photovoltaic Cells—A Review and the Perspective of Pulsating Flow Cooling," *Energies*, vol. 16, no. 6, p. 2842, Mar. 2023.

[36] A. Legala and X. Li, "Hybrid data-based modeling for the prediction and diagnostics of Li-ion battery thermal behaviors," *Energy AI*, vol. 10, p. 100194, Nov. 2022.

[37] F. Hu, C. Dong, L. Tian, Y. Mu, X. Yu, and H. Jia, "CWGAN-GP with residual network model for lithium-ion battery thermal image data expansion with quantitative metrics," *Energy AI*, vol. 16, p. 100321, May 2024.

Qing Qin received a BEng (Hons.) degree in Automotive Engineering from Coventry University, Coventry, UK, in 2018, and an MSc degree in Automotive Engineering from Cranfield University, Bedford, UK, in 2019. She received a PhD degree in Aerospace from Cranfield University, Bedford, UK, in 2023, focusing on Poisson's ratio metamaterial studies. She is currently a Research Fellow at Cranfield University, Bedford, UK, focusing on battery thermal management. Her main research interests include thermal management, renewable energy, smart structures, and metamaterials.

Patrick Chi-Kwong Luk (Senior Member, IEEE) was born in Hong Kong. He received a Higher Diploma degree (Hons.) from The Hong Kong Polytechnic University (PolyU), Hong Kong, in 1983, an M.Phil. degree from The University of Sheffield, U.K., in 1989, and a PhD degree from the University of South Wales, U.K., in 1992, all in electrical engineering. From 1981 to 1983, he was an Engineer Trainee at GEC, Hong Kong. After graduation, he worked as an Applications Engineer at Polytek Engineering Company, Hong Kong. In 1986, he became a Senior Researcher with the Industrial Centre at PolyU. From 1988 to 2001, he held research and academic positions at the University of South Wales, Robert Gordon University, and the University of Hertfordshire, U.K. He joined Cranfield University, Cranfield, U.K., in 2002, where he is currently the Chair Professor in Electrical Engineering. He has authored over 240 publications in power electronics and motor drives. He holds or has held numerous professional and voluntary positions, including Chairman of the IEEE UK&I Power Electronics Chapter, Associate Editor of IEEE Transactions on Power Electronics, and Distinguished Lecturer for the IEEE Vehicular Technology Society. His research interests include electrical drives, high-frequency electronics, and their applications in transportation and energy conversion

Zhenhua Luo received his BSc in nanotechnology in 2006, and PhD degrees in materials science and engineering in 2011, at the University of New South Wales, Australia.
From 2013 to 2016, he was a Research Fellow at University of Southampton, UK. Since 2016, he has been an academic at Cranfield University, UK, and is currently a Senior Lecturer in Energy Storage and Harvesting. He has published over 50 research articles and 3 patents. His current research interests include renewable energy and energy harvesting, focusing on piezoelectric and thermoelectric, and solar-to-hydrogen generation. He is currently a steering board member of the UK Energy Harvesting Network.
Dr Luo was a recipient of the Innovate UK ICURe award in 2019, and the UK universities' Award for Excellence in Hydrogen Research and Innovation in 2024. He has also been nominated for the Earthshot Prize in 2024.

Battery thermal management for microchannel cooling system with scanning flow method

Qin, Qing

2025-02

Qin Q, Luo Z, Luk P. (2025) Battery thermal management for microchannel cooling system with scanning flow method. IEEE Transactions on Transportation Electrification. Volume 11, Issue 1, February 2025, pp. 2840-2850

https://doi.org/10.1109/TTE.2024.3429202